Tailor-Made Magnetic Fe_3O_4@mTiO_2 Microspheres with a Tunable Mesoporous Anatase Shell for Highly Selective and Effective Enrichment of Phosphopeptides

Wan-Fu Ma,[†,§] Ying Zhang,[‡,§] Lu-Lu Li,[‡] Li-Jun You,[†] Peng Zhang,[†] Yu-Ting Zhang,[†] Ju-Mei Li,[†] Meng Yu,[†] Jia Guo,[†] Hao-Jie Lu,[‡,*] and Chang-Chun Wang[†,*]

[†]State Key Laboratory of Molecular Engineering of Polymers and Department of Macromolecular Science, Laboratory of Advanced Materials, Fudan University, Shanghai 200433, People's Republic of China and [‡]Department of Chemistry and Institutes of Biomedical Sciences, Fudan University, Shanghai 200032, People's Republic of China. [§]Both authors contributed equally to this work.

ABSTRACT Selective enrichment of phosphoproteins or phosphopeptides from complex mixtures is essential for MS-based phosphoproteomics, but still remains a challenge. In this article, we described an unprecedented approach to synthesize magnetic mesoporous Fe_3O_4@mTiO_2 microspheres with a well-defined core/shell structure, a pure and highly crystalline TiO_2 layer, high specific surface area (167.1 m^2/g), large pore volume (0.45 cm^3/g), appropriate and tunable pore size (8.6−16.4 nm), and high magnetic susceptibility. We investigated the applicability of Fe_3O_4@mTiO_2 microspheres in a study of the selective enrichment of phosphopeptides. The experiment results demonstrated that the Fe_3O_4@mTiO_2 possessed remarkable selectivity for phosphopeptides even at a very low molar ratio of phosphopeptides/non-phosphopeptides (1:1000), large enrichment capacity (as high as 225 mg/g, over 10 times as that of the Fe_3O_4@TiO_2 microspheres), extreme sensitivity (the detection limit was at the fmol level), excellent speed (the enrichment can be completed in less than 5 min), and high recovery of phosphopeptides (as high as 93%). In addition, the high magnetic susceptibility allowed convenient separation of the target peptides by magnetic separation. These outstanding features give the Fe_3O_4@mTiO_2 composite microspheres high benefit for mass spectrometric analysis of phosphopeptides.

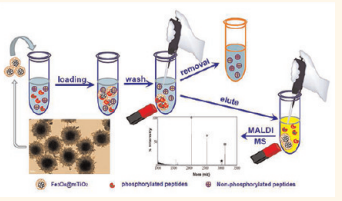

KEYWORDS: mesoporous microspheres · magnetic clusters · titanium oxide · enrichment of phosphopeptides · mass spectrometric analysis

Magnetic composite microspheres have been extensively investigated, due to their wide range of current and potential applications in the biomedical field.[1−11] They allow mechanical sorting, trafficking, and other forms of micromanipulation to be easily performed in biological systems; this is achieved simply *via* the application of an external magnetic field, while the particles are viewed and followed using MRI tomographic methods.[12−15] Recently, the application of magnetic composite microspheres in proteomics research has received much attention.[16−21] Reversible protein phosphorylation is one of the most important protein post-translational modifications; it plays a vital role in regulating many complex biological processes such as cellular growth, division, and signaling transduction, and investigations into this process are of keen interest in the field of proteomics.[22−24] Mass spectrometry (MS) has become the most important and powerful tool for the analysis of protein phosphorylation, due to its ultrahigh sensitivity, its wide dynamic range, and its superior speed in analyzing mixtures. However, the identification and characterization of phosphoproteins remains one of the most challenging tasks in contemporary proteomic research, due to their low dynamic stoichiometry. The selective enrichment of phosphoproteins or phosphopeptides from complex mixtures is therefore essential for MS-based phosphoproteomics.

Of the various enrichment strategies, immobilized metal affinity chromatography (IMAC)—which relies on the affinity of the phosphate groups to metal ions immobilized on a matrix—is the most commonly used technique to fish the phosphorylated peptides out of the pool of predominantly non-phosphorylated peptides. In recent years, metal oxide nanoparticles such as TiO_2, ZrO_2, and HfO_2 have been demonstrated to be more specific in the trapping of phosphoproteins/phosphopeptides than conventional IMAC; this is because such

* Address correspondence to ccwang@fudan.edu.cn; luhaojie@fudan.edu.cn.

Received for review December 22, 2011 and accepted March 27, 2012.

Published online March 27, 2012
10.1021/nn3009646

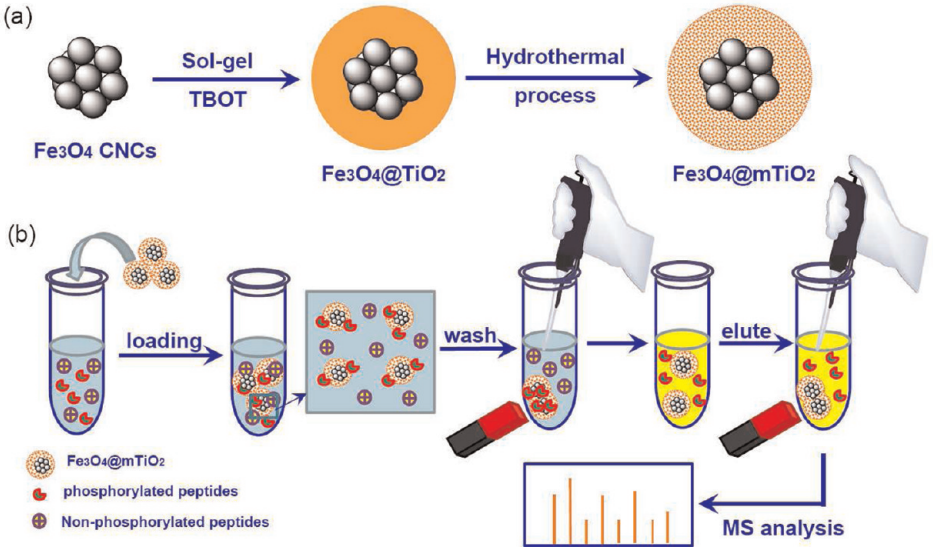

Scheme 1. Schematic illustration of (a) synthetic procedure for the fabrication of the mesoporous Fe_3O_4@mTiO_2 core/shell microspheres and (b) the selective process for the enrichment of phosphorylated peptides using Fe_3O_4@mTiO_2 microspheres and magnetic separation.

oxides display more specific and reversible chemisorption of phosphate groups on their amphoteric surface.[25−27] In particular, recent advances in mesoporous TiO_2 synthesis have led to the development of the current state of the art phosphate-adsorbing materials, which have a higher enrichment capacity and better selectivity than solid oxides.[28−30] However, when the phosphopeptide-bound materials were harvested using centrifugation, high-molecular-weight non-phosphopeptides were sedimented at high rotation speeds (up to 16 000 rpm). We therefore formulated a rational design to combine magnetic nanomaterials with mesoporous TiO_2, with the aim of achieving the simple and efficient separation of the phosphopeptides from the peptide mixture in the harvesting step.

Herein, for the first time, we present a novel method to fabricate well-defined core/shell microspheres with an Fe_3O_4 colloidal nanocrystal cluster as a core and a mesoporous crystalline TiO_2 as a shell (Fe_3O_4@mTiO_2). These composite nanomaterials were investigated in a study of the selective enrichment of phosphopeptides. The Fe_3O_4@mTiO_2 microspheres were designed to possess the following features: (1) a pure and highly crystalline TiO_2 layer showing a remarkable selectivity toward phosphopeptides; (2) a relatively large pore volume and appropriate pore size, which ensured a large enrichment capability and a high mass transport efficiency by allowing the enrichment time to be shortened and a high recovery efficiency to be achieved; (3) a high-magnetic-response Fe_3O_4 core, allowing separation to be conveniently performed, by the simple application of an external magnetic field. These Fe_3O_4@mTiO_2 composite microspheres with the aforementioned unique properties are anticipated to become sustainable reservoirs for the selective enrichment of phosphopeptides; this would be highly beneficial for mass spectrometric analysis.

RESULTS AND DISCUSSION

The protocol for the synthesis of the Fe_3O_4@mTiO_2 composite microspheres is illustrated in Scheme 1a. A compact TiO_2 layer was deposited directly on the surface of magnetite colloidal nanocrystal clusters (MCNCs) using a sol−gel method. They were then subjected to a hydrothermal treatment, which led to the formation of a tailor-made mesoporous TiO_2 shell.

Briefly, the citrate-stabilized MCNCs were prepared using a modified solvothermal route.[31,32] The obtained MCNCs had a spherical shape with a mean diameter of about 280 nm (Figure 1a). A high-resolution TEM (HRTEM) image (Figure S1) further reveals that the microspheres are composed of nanocrystals with a size of about 7−11 nm. The average crystallite size in these microspheres can be further calculated by the strongest peak at 25.2° in the PXRD spectrum (Figure 2a) using Scherrer's formula; the data were around 10.4 nm. The thermogravimetric analysis (TGA) of MCNCs (Figure 3a) indicates that the content of the citrate stabilizer is as high as 18 wt %, which suggests that the citrate molecules are not only at the surface but also located between the magnetite nanocrystals forming the MCNC cores.

The carboxyl groups provided by the citrate stabilizer gave the MCNCs outstanding dispersibility in many polar solvents and also adsorbed positive ammonium ions, which further drew the negatively charged $\equiv TiO^-$ species together, and thereby facilitated the direct deposition of titania *via* the sol−gel process.[33,34] The coating reaction was thoroughly

investigated by varying the feeding amounts of ammonia and tetrabutylorthotitanate (TBOT) and the volume ratio of ethanol/acetonitrile. As is evident from the TEM image shown in Figure 1b, a well-defined core/shell structure was produced. An energy dispersive X-ray (EDX) spectrum was recorded to identify the composition of the resulting microspheres (Figure S2). Ti, Fe, and O were the three main elements found, indicating that the obtained microspheres were composed of the target materials. This confirmed that it was possible for well-structured Fe_3O_4@TiO_2 materials to be obtained. The hydrodynamic diameter (D_h) of MCNCs and Fe_3O_4@TiO_2 represented in Figure S3a and S3b provides additional evidence for the successful coating; the average D_h of MCNCs and Fe_3O_4@TiO_2 is 314 and 558 nm, respectively (close to the size measured by TEM), and the narrow size distributions (the polydispersity index for MCNCs and Fe_3O_4@TiO_2 is 0.097 and 0.071, respectively) indicate that they all have a good dispersibility in water. In addition, the TiO_2 shell appeared to be continuous and compact in terms of its structure; the possibility of tuning the thickness was afforded by varying the amount of TBOT that was fed into the reaction. In contrast to the known strategies for the synthesis of TiO_2 composite microspheres,

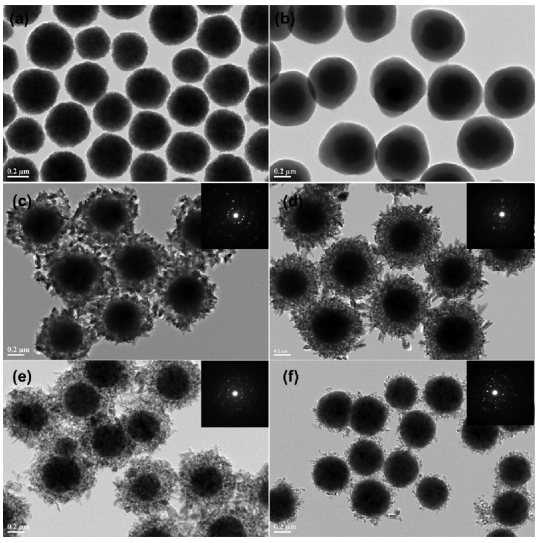

Figure 1. Representative TEM images of (a) MCNCs and (b) Fe_3O_4@TiO_2 and Fe_3O_4@mTiO_2, prepared under different ethanol/deionized water ratios of (c) 60:0, (d) 40:20, (e) 20:40, and (f) 0:60. (All scale bars are 200 nm.)

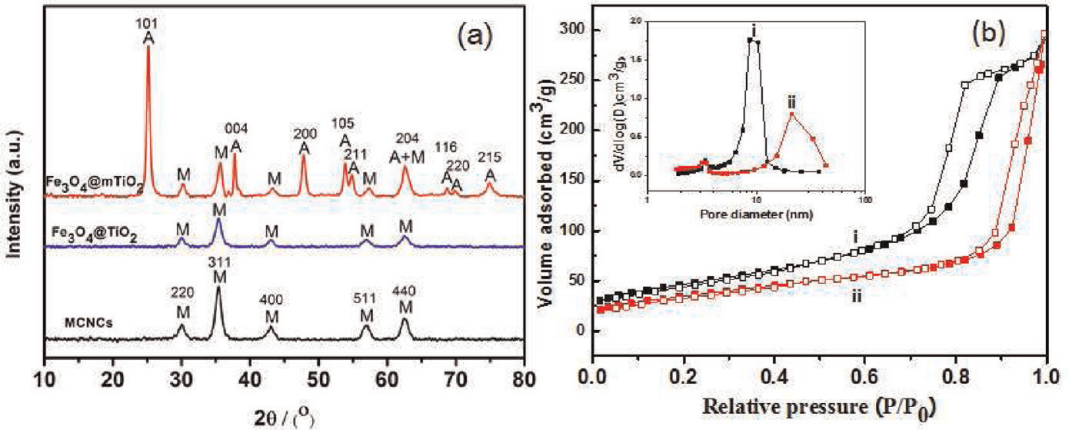

Figure 2. (a) XRD patterns for MCNCs, Fe_3O_4@TiO_2, and Fe_3O_4@mTiO_2, (b) nitrogen adsorption−desorption isotherms (■ = adsorption, □ = desorption) and BJH pore-size distribution curves (inset) for Fe_3O_4@mTiO_2 prepared with an $NH_3 \cdot H_2O$ dosage of (i) 0 and (ii) 3 mL.

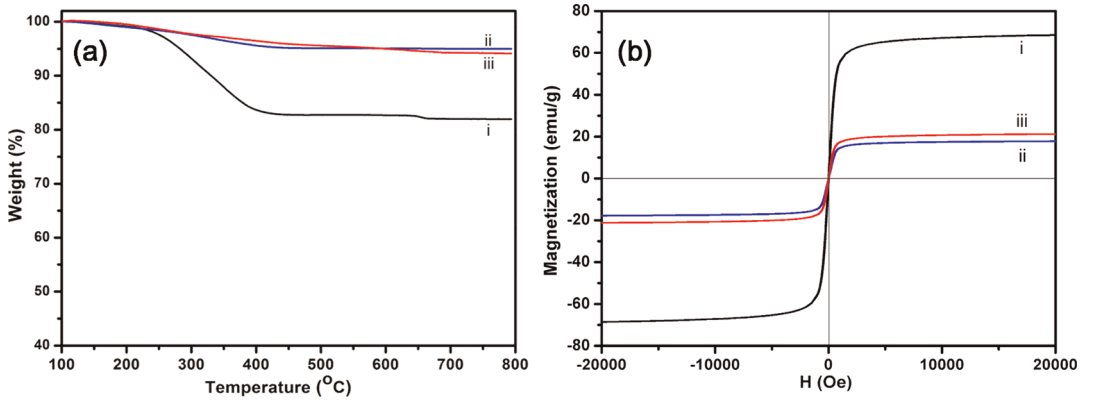

Figure 3. (a) TGA curves and (b) magnetic hysteresis curves of (i) MCNCs, (ii) Fe_3O_4@TiO_2, and (iii) Fe_3O_4@mTiO_2 (prepared with 40:20 volume ratio of ethanol to water and 3 mL of $NH_3 \cdot H_2O$).

this facile approach allowed the growth of TiO_2 over Fe_3O_4 colloids to be achieved without the use of any intermediate components (for example, an SiO_2 sandwich layer is typically used to give higher accessibility to TiO_2 precursors).[35−37]

The magnetic properties of MCNCs and the Fe_3O_4@TiO_2 composite microspheres were studied using a vibrating sample magnetometer (Figure 3b). The magnetic hysteresis curves of MCNCs and Fe_3O_4@TiO_2 showed that the two kinds of microspheres have no obvious remanence or coercivity at 300 K, indicating that they all possess a superparamagnetic feature. The superparamagnetism is coming from the small nanocrystals in the MCNC cores, which behave as superparamagnets. Additionally, the citrate stabilizer may also screen the dipolar interactions between the nanocrystals so as to greatly decrease the coercivity. A similar result could be found in the previous literature.[38] As a control, the saturation magnetization (Ms) value of the MCNCs was measured; it reached 68.4 emu/g. Upon coating of a 100 nm thick amorphous TiO_2 layer, the Ms value for the Fe_3O_4@TiO_2 microspheres was reduced to 17.8 emu/g. Accordingly, the TiO_2 content of the composite microspheres was estimated to be as high as 74 wt %; this estimate was performed by comparing the Ms values before and after coating of the TiO_2 layers, which agrees well with the calculation (72.2 wt %) from the thermogravimetric measurements (Figure 3a). The high TiO_2 content was responsible for the abundance of binding sites on the microspheres that were available to anchor the phosphopeptides. The composite microspheres could be separated from the solution (VH_2O/VCH_3CN, 1:1) in only 30 s when the magnetic field was applied (Figure S4a). The specific surface area of the Fe_3O_4@TiO_2 microspheres was characterized using nitrogen adsorption−desorption measurements (Figure S5). A typical micropore isotherm curve was obtained, and the average pore size calculated using the Horvath−Kawazoe model[39] was approximately 0.7 nm. This was unfortunately too small to allow the infiltration of the phosphopeptides (the diameter of gyration of the investigated phosphopeptides was calculated to be about 2−3 nm).

The mesoporous TiO_2 shell was created by hydrothermally treating the as-synthesized Fe_3O_4@TiO_2 microspheres in a mixed ethanol/water solvent, with $NH_3 \cdot H_2O$ as porosity modifier. TEM images of the Fe_3O_4@mTiO_2 microspheres prepared at various ethanol/water volume ratios (in a total volume of 60 mL) are shown in Figure 1c to f. The feeding amounts of Fe_3O_4@TiO_2 and $NH_3 \cdot H_2O$ were maintained at a constant level (50 mg and 3 mL), and the volume ratios of ethanol to water were varied (the samples had ratios of 60:0, 40:20, 20:40, and 0:60), producing the different samples displayed in Figure 1c, d, e, and f, respectively. The TiO_2 shells appeared to have different

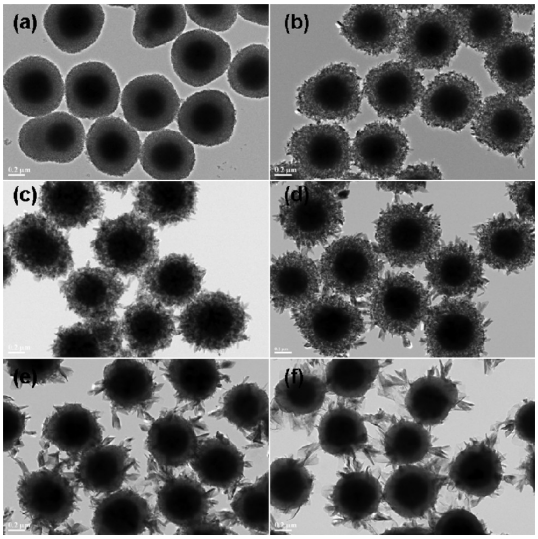

Figure 4. (a−f) Representative TEM images of Fe_3O_4@mTiO_2 prepared with different amounts of $NH_3 \cdot H_2O$: (a) 0 mL, (b) 1 mL, (c) 2 mL, (d) 3 mL, (e) 4 mL, (f) 6 mL. (All scale bars are 200 nm.)

textures; more porous-looking shells were produced as the volume ratios were changed from 60:0, to 40:20, to 20:40 under otherwise identical conditions. Without ethanol in the reaction, the TiO_2 shell was almost nonexistent, leaving only a small remainder on the MCNCs (Figure 1f). Selected-area electron diffraction (SAED) patterns recorded from a certain shell area for individual microspheres revealed that the TiO_2 shells prepared under these four reaction conditions were all polycrystalline and were constructed from many TiO_2 nanocrystals (see insets in Figure 1c−f). Interestingly, the crystallization and pore-creation processes took place simultaneously during the hydrothermal treatment.

In addition to the role played by the solvents, we also found that the concentration of ammonia had a great effect on the formation of the structures in the Fe_3O_4@mTiO_2 microspheres, which was achieved by adjusting the alkalinity of the solution and thereby tuning the crystal process.[40] Representative TEM images are shown in Figure 4 for the products prepared with different amounts of $NH_3 \cdot H_2O$, with a constant 40:20 volume ratio of ethanol to water. Even with no $NH_3 \cdot H_2O$ in the solution, the TiO_2 shell seemed to be porous. When the amount of $NH_3 \cdot H_2O$ was increased, the porosity of the TiO_2 shell was enhanced accordingly, as confirmed in Figure 4b, c, and d. However, it is surprising that as the amount of $NH_3 \cdot H_2O$ was increased to over 3 mL, numerous sheet-shaped crystals became bound onto the peripheral surface of the TiO_2 shell (Figure 4e and f). We believe that the excess $NH_3 \cdot H_2O$ did not facilitate the formation of the homogenously structured porous shell, but promoted the crystal growth of the surface; this was further confirmed in the SEM images (Figure 5). The phase evolution of the

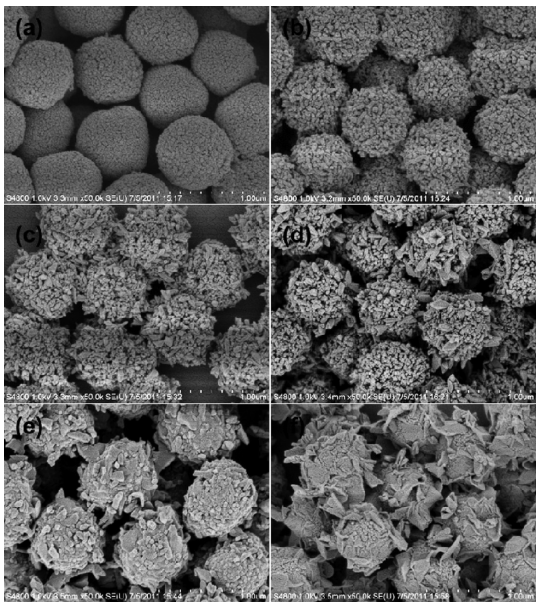

Figure 5. (a–f) Representative SEM images of Fe_3O_4@mTiO_2 core/shell microspheres prepared under different $NH_3 \cdot H_2O$: (a) 0 mL, (b) 1 mL, (c) 2 mL, (d) 3 mL, (e) 4 mL, (f) 6 mL. (All scale bars are 1 μm.)

TiO_2 in the shell was closely monitored as a function of reaction time, to reveal the process of crystalline conversion (Figures S6 and S7). It can be seen that the sheet-like nanocrystals on the shells were just formed after 8 h; as the reaction continued, the crystallization extended into the internal layer to yield a considerable amount of nanocrystals, and this was accompanied by the continuous growth of the superficial sheet crystals.

The crystalline structure of the composite Fe_3O_4@mTiO_2 microspheres was rigorously investigated using powder X-ray diffraction (PXRD, Figure 2a). Prior to the crystallization treatment of the TiO_2 shells, the Fe_3O_4@TiO_2 microspheres showed a simple PXRD pattern, which could be well ascribed to the typical cubic structure of Fe_3O_4 (JCPDS 19-629). No characteristic TiO_2 crystal peaks were detected, which was indicative of an amorphous TiO_2 shell formed around the MCNC core. After hydrothermal treatment for 20 h, the PXRD pattern for the synthesized Fe_3O_4@mTiO_2 microspheres was noticeably different from the former pattern. In addition to the diffraction peaks that were preserved due to the Fe_3O_4 component, the other peaks (marked with "A" in the spectrum) could be well indexed to the typical crystallographic planes of an anatase-phase TiO_2. This confirmed again the occurrence of a structural transition in the TiO_2 shell, from amorphous to crystalline phase. The average crystal sizes in the shells of the composite microspheres were calculated using Scherrer's formula. The strongest peak at 25.2° in the PXRD spectrum was used, and the average nanocrystal size in the TiO_2 shells that were synthesized with 3 mL of $NH_3 \cdot H_2O$ was about 18.7 nm. In the other samples, which were synthesized using 2, 1, and 0 mL of $NH_3 \cdot H_2O$, the grain sizes of the TiO_2 nanocrystals in the shells showed a decreasing tendency, which were further confirmed by the HRTEM images shown in Figure S8; the peaks for these samples corresponded to nanocrystals with sizes of 15.3, 13.4, and 9.8 nm. This showed that NH_3 promoted the size evolution of the TiO_2 nanocrystals during their structural transition; it is possible that the presence of excess $NH_3 \cdot H_2O$ in the synthesis led to more pronounced orientational growth, which in turn led to the formation of the larger sheet-shaped crystals fixed on the outmost layer, as shown in Figure 4e and f.

The well-structured Fe_3O_4@mTiO_2 microspheres synthesized with $NH_3 \cdot H_2O$ amounts of 0 and 3 mL under the 40:20 volume ratio of ethanol to water were subjected to further study of their porosity, by means of nitrogen sorption analysis performed at 77 K. As shown in Figure 2b, the two kinds of Fe_3O_4@mTiO_2 exhibited typical type IV gas sorption isotherms, which were indicative of the mesoporous character that both samples showed. According to calculations made using the BET model,[41] the Fe_3O_4@mTiO_2 materials synthesized without and with the addition of $NH_3 \cdot H_2O$ (3 mL) resulted in specific surface areas of 167.1 and 126.2 m^2/g, respectively, and similar pore volumes of 0.45 cm^3/g. Their corresponding pore-size distributions were evaluated using the Barrett–Joyner–Halenda (BJH) model,[42] and the populations were found to be centered at 8.6 and 16.4 nm (Figure 2b, inset), respectively. Considering these results together with the small sizes of the TiO_2 nanocrystals (as calculated from the PXRD patterns) leads to a possible hypothesis; the mesoporosity might result from a number of nanocrystals stacking with each other to form a shell, simultaneously producing tiny slits between the neighboring primary nanocrystals in the shells. The Fe_3O_4@mTiO_2 synthesized with 3 mL of $NH_3 \cdot H_2O$ showed a reduced surface area and larger pore sizes; this could be explained to result from the larger TiO_2 nanocrystals in their shells. Even with impaired porosity, this sample showed larger pore sizes than the others; the larger pore size is conducive to the permeation of peptides during the selective enrichment. The magnetic properties of this larger-pore-size sample were assessed, to determine whether a fast separation of the particles (out of the medium) could be performed. The magnetic hysteresis curve shows an Ms of 21.2 emu/g, slightly higher than that of pristine Fe_3O_4@TiO_2 (17.8 emu/g) (see Figure 3b), which also agrees well with the TGA result (Figure 3a). In the practice separation test, the Fe_3O_4@mTiO_2 composite microspheres could be completely attracted within only 15 s (Figure S4b). Such a short separation time reflects the potential of these particles for the rapid isolation of target peptides. The average D_h of these particles (Figure S3c) of 632 nm (a few larger than Fe_3O_4@TiO_2) and the narrow size distribution (the PDI

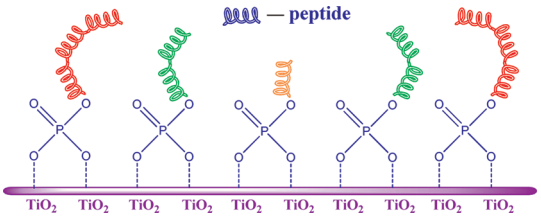

Scheme 2. Schematic illustration of the interaction between the phosphoric acid group of phosphopeptides and TiO_2.

for Fe_3O_4@mTiO_2 is 0.062) further confirm that they are dispersed as single spheres rather than aggregating in solution, which is essential for the following enrichment experiments.

TiO_2 has attracted considerable attention as a novel material for the enrichment of phosphopeptides from complex mixtures. Phosphopeptides can be captured by TiO_2 through bridging bidentate bonds between the phosphoric acid group of phosphopeptides and TiO_2 (Scheme 2),[43] which are formed between the phosphate anions and the metal oxide surface. Here, the enrichment selectivity and capacity of Fe_3O_4@mTiO_2 toward phosphopeptides were investigated using the tryptic digest of a standard phosphoprotein, β-casein. In a typical enrichment procedure, the β-casein digest was first dissolved in a 100 μL loading buffer consisting of 50% acetonitrile containing 1% trifluoroacetic acid (TFA) and was then incubated with Fe_3O_4@mTiO_2. The Fe_3O_4@mTiO_2 and captured phosphopeptides were then separated from the mixed solution, using an external magnetic field. The collected products were then washed with the loading buffer, to remove any nonspecifically adsorbed peptides. Finally, the trapped phosphopeptides were eluted with 10 μL of 5% $NH_3 \cdot H_2O$, and 1 μL of this solution was used for MALDI-TOF MS analysis. Figure S9 shows the mass spectra for the peptides before and after the Fe_3O_4@mTiO_2 enrichment. After selective enrichment, signals could be clearly observed for all three phosphopeptides (at *m/z* 2061.83, 2556.09, and 3122.27) (Figure S9b). As a control, the same amount of β-casein digest was analyzed in the absence of the pretreatment procedure. The obtained spectrum was dominated by non-phosphopeptides (Figure S9a), and their presence led to a low signal-to-noise ratio for the phosphopeptides. This result confirmed the enrichment selectivity of Fe_3O_4@mTiO_2 for phosphopeptides.

To further evaluate their ability to capture phosphopeptides in complex samples, the Fe_3O_4@mTiO_2 microspheres were applied to trap phosphopeptides in mixtures of a tryptic digest of β-casein and bovine serum albumin (BSA) (with a molar ratio of 1:1000); the Fe_3O_4@TiO_2 microspheres with amorphous TiO_2 shells were used as a reference comparison. As shown in Figure 6a, no phosphopeptides were detected before enrichment, due to the presence of large amounts of

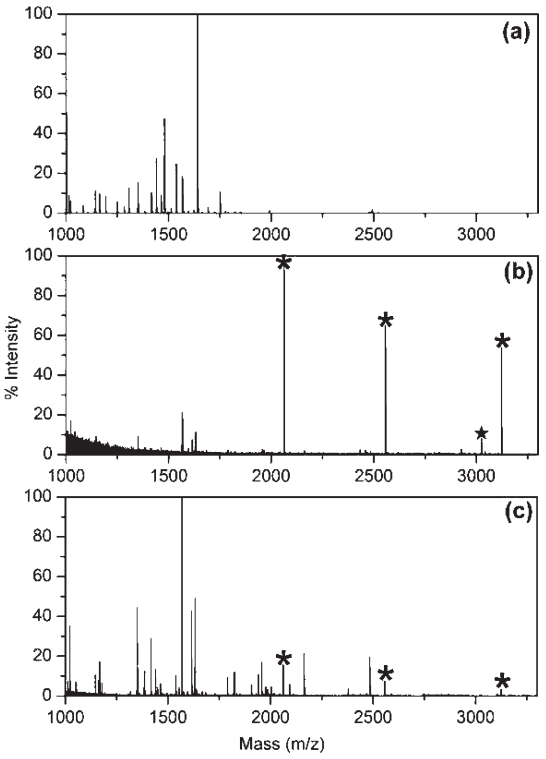

Figure 6. MALDI mass spectra of the tryptic digest mixture of β-casein and BSA (with a molar ratio of β-casein to BSA of 1:1000). (a) Direct analysis and analysis after enrichment using (b) Fe_3O_4@mTiO_2 and (c) Fe_3O_4@TiO_2. "*" and "★" indicate phosphorylated peptides and their dephosphorylated counterparts, respectively.

non-phosphopeptides (from the BSA). When the Fe_3O_4@TiO_2 microspheres with amorphous shells were used, the efficacy of the enrichment was inferior (Figure 6c), with lower phosphopeptide intensities and non-phosphopeptide peaks dominating the spectrum. However, after incubation with Fe_3O_4@mTiO_2, all three phosphopeptides could be easily detected, with a very clean background in the mass spectrum (Figure 6b). To the best of our knowledge, this is the highest enrichment selectivity hitherto observed; we achieved an order-of-magnitude improvement over the recently reported mesoporous TiO_2 synthesized using a surfactant-aided assembly route,[29] and the selectivity is also much better than the previously reported Fe_3O_4@TiO_2 nanoparticles.[44−46] We attribute this unprecedented selectivity of the Fe_3O_4@mTiO_2 to the 100% purity and high crystallinity of the TiO_2 composition, with no impurity moieties left within the shells.

With their exceptional porosity in mind, we investigated the enrichment capacity of the Fe_3O_4@mTiO_2 composite microspheres toward β-casein phosphopeptides. Equivalent amounts of Fe_3O_4@mTiO_2 and Fe_3O_4@TiO_2 were used to selectively enrich phosphopeptides from β-casein; a series of samples using varying amounts of phosphopeptides were prepared. After the samples were loaded, the flow-through fractions were analyzed using MALDI-TOF MS. When the

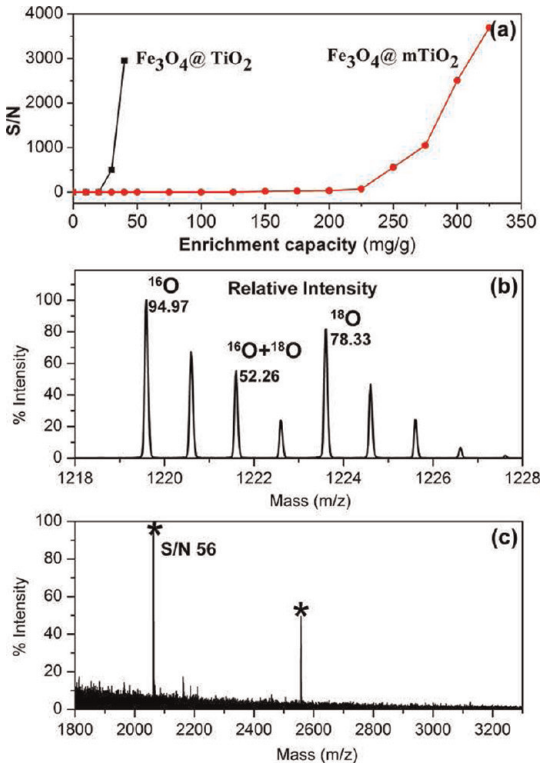

Figure 7. (a) Enrichment capacity analysis of Fe_3O_4@$mTiO_2$ and Fe_3O_4@TiO_2; (b) MALDI mass spectrum of phosphopeptide pSADGQHAGGLVK (a mixture of unlabeled enriched and an equal amount of ^{18}O-labeled unenriched, used as a control); (c) MALDI mass spectrum of a tryptic digest of β-casein (0.1 nM, 100 μL), after enrichment.

total amount of β-casein was lower than the capacity of the materials, the phosphopeptides could not be detected. Once the phosphopeptide's signal was detected by MALDI-TOF MS—meaning that the material could not capture all of the phosphopeptides at the concentration in question—the enrichment capacity of the material could be estimated. As illustrated in Figure 7a, the enrichment capacity of Fe_3O_4@TiO_2 was 20 mg/g. The mesoporous Fe_3O_4@$mTiO_2$ microspheres showed enrichment capacities as high as 225 mg/g, nearly 10 times higher than that of Fe_3O_4@TiO_2. As detailed above, the porous structure of the Fe_3O_4@$mTiO_2$ microspheres featured a large pore volume (0.45 cm^3/g) and a suitable mesopore size (16.4 nm), which ensured the infiltration of the peptides into the cavities between the primary TiO_2 nanocrystals (and thereby produced behavior that was clearly different from that of the microporous Fe_3O_4@TiO_2 microspheres). Also by virtue of the large pore volume, the enrichment can be completed in less than 5 min.

The postenrichment recovery of phosphopeptides from Fe_3O_4@$mTiO_2$ was investigated. A certain amount of standard phosphopeptide (pSADGQHAGGLVK) was divided equally into two parts. The first part was treated with immobilized trypsin (homemade) in $H_2{}^{18}O$, which produced a 4 Da mass increase by introducing two ^{18}O atoms at the C-termini of the peptides. The second part was applied in our trap-and-release strategy. By mixing the two parts, we could profile the product with MS to make a comparative study of the abundances of the phosphopeptides from different oxygen isotopes, according to the peak relative intensities.[47] As the MALDI mass spectrum in Figure 7b reveals, the recovery of phosphopeptides from the Fe_3O_4@$mTiO_2$ was as high as 93%. Furthermore, the high detection sensitivity of this approach was demonstrated, as illustrated in the MALDI mass spectrum shown in Figure 7c. The targeted phosphopeptide (*m/z* 2061.83) could be easily enriched and could be detected at a signal-to-noise ratio of 56, even when the total amount of β-casein was decreased to only 10 fmol. This indicated that the detection limit of this method was at the fmol level. These tests lead us to believe that the Fe_3O_4@$mTiO_2$ microspheres act as an ideal adsorbent for phosphopeptides with remarkable selectivity, extreme sensitivity, large capacity, excellent speed, and sustainable enrichment recovery.

CONCLUSION

In summary, we have presented a new facile, repeatable, and mass spectrometry-friendly synthetic route for the preparation of magnetic mesoporous Fe_3O_4@$mTiO_2$ core/shell microspheres with a magnetite core and a homogeneous mesoporous crystalline TiO_2 shell. The characterization results showed that the ethanol/water volume ratio and the amount of $NH_3 \cdot H_2O$ had large effects on the structure of the obtained Fe_3O_4@$mTiO_2$ microspheres. The phosphopeptide enrichment experiments confirmed that the Fe_3O_4@$mTiO_2$ microspheres had excellent selectivity for phosphopeptides. This research has important implications for the preparation of other similar core/shell magnetic mesoporous nanomaterials. We also believe that these mesoporous Fe_3O_4@$mTiO_2$ microspheres have great potential for photocatalysis and other biomedical applications.

EXPERIMENTAL SECTION

Materials. Iron(III) chloride hexahydrate ($FeCl_3 \cdot 6H_2O$), ammonium acetate (NH_4OAc), ethylene glycol, anhydrous ethanol, trisodium citrate dehydrate, and aqueous ammonia solution (25%) were purchased from Shanghai Chemical Reagents Company and used as received. β-Casein, bovine serum albumin (95%), 2,5-dihydroxybenzoic acid (2,5-DHB, 98%), ammonium bicarbonate (ABC, 99.5%), and 1,1-(tosylamido)-2-phenylethyl chloromethyl ketone (TPCK)-treated trypsin (E.G 2.4.21.4) were purchased from Sigma (St.Louis, MO, USA).

Acetonitrile (ACN, 99.9%) and trifluoroacetic acid (99.8%) were purchased from Merck (Darmstadt, Germany). Phosphoric acid (85%) was purchased from Shanghai Feida Chemical Reagents Ltd. (Shanghai, China). Matrix DHB was dissolved in an acetonitrile (ACN)/water (50/50, v/v) solution containing 1% H_3PO_4 by keeping DHB at 10 mg/mL. Deionized water (18.4 MΩ cm) used for all experiments was obtained from a Milli-Q system (Millipore, Bedford, MA, USA). Field-emission transmission electron microscopy (FE-TEM) images were taken on a JEM-2100F transmission electron microscope at an accelerating voltage of 200 kV. Samples dispersed at an appropriate concentration were cast onto a carbon-coated copper grid. Field-emission scanning electron microscopy (FE-SEM) was performed with a Hitachi S-4800 scanning electron microscope at an accelerating voltage of 20 kV. Samples dispersed at an appropriate concentration were cast onto a glass sheet at room temperature and sputter-coated with gold. Magnetic characterization was carried out with a vibrating sample magnetometer on a Model 6000 Physical Property Measurement System (Quantum, USA) at 300 K. XRD patterns were collected on an X'Pert Pro (Panalytical, The Netherlands) diffraction meter with Cu KR radiation at λ = 0.154 nm operating at 40 kV and 40 mA. Nitrogen adsorption−desorption measurements were performed on an ASAP2020 (Micromeritics, USA) accelerated surface area analyzer at 77 K. Before measuring, the samples were degassed in a vacuum at 120 °C for at least 6 h.

Preparation of MCNCs Stabilized by Citrate. The magnetite colloidal nanocrystal clusters were prepared through a modified solvothermal reaction. Typically, 1.350 g of $FeCl_3 \cdot 6H_2O$, 3.854 g of NH_4Ac, and 0.400 g of sodium citrate were dissolved in 70 mL of ethylene glycol. The mixture were stirred vigorously for 1 h at 170 °C to form a homogeneous black solution and then transferred into a Teflon-lined stainless-steel autoclave (100 mL capacity). The autoclave was heated at 200 °C and maintained for 16 h; then it was cooled to room temperature. The black product was washed with ethanol and collected with the help of a magnet. The cycle of washing and magnetic separation was repeated several times. The final product was dispersed in ethanol for further use.

Preparation of Fe_3O_4@TiO_2 Core/Shell Microspheres. The Fe_3O_4@TiO_2 core/shell microspheres were synthesized by directly coating a TiO_2 layer on the surface of MCNCs in the mixed solvent of ethanol and acetonitrile at room temperature by hydrolyzing TBOT in the presence of ammonia. Briefly, about 50 mg of the as-prepared MCNCs was dispersed in a mixed solvent containing 90 mL of ethanol and 30 mL of acetonitrile with the aid of ultrasound and then mixed with 0.5 mL of $NH_3 \cdot H_2O$ at room temperature. Finally, 1 mL of TBOT was added to the above suspension under stirring. After reacting for 1.5 h, the products were collected by magnetic separation and washed with ethanol and acetonitrile several times.

Preparation of Fe_3O_4@mTiO_2 Core/Shell Microspheres. The mesoporous TiO_2 shells were achieved by treating the obtained Fe_3O_4@TiO_2 microspheres with a hydrothermal method. Typically, 50 mg of the as-synthesized Fe_3O_4@TiO_2 microspheres was dispersed in 60 mL of mixed solvent of ethanol and deionized water, and then a certain amount of $NH_3 \cdot H_2O$ was added to the above suspension. The mixture was then transferred to a Teflon-lined stainless-steel autoclave (100 mL capacity). The autoclave was heated at 160 °C and maintained for 20 h. Then it was cooled to room temperature, and the black product was washed with ethanol and collected with the help of a magnet.

Preparation of Tryptic Digest of Standard Proteins. β-Casein and BSA were each dissolved in 25 mM ABC at pH 8.0 (1 mg/mL for each protein) and denatured by boiling for 10 min. Protein solutions were then incubated with trypsin at an enzyme/substrate ratio of 1:40 (w/w) for 12 h at 37 °C to produce proteolytic digests, respectively. The tryptic peptide mixtures were stored at −20 °C until further use.

Selective Enrichment of Phosphopeptides with Fe_3O_4@TiO_2 and Fe_3O_4@mTiO_2 Microspheres. The obtained Fe_3O_4@TiO_2 or Fe_3O_4@mTiO_2 was first washed with ethanol three times and then suspended in deionized water at 10 mg/mL. Tryptic digests of β-casein and BSA was dissolved in 200 μL of loading buffer (50% ACN containing 1% TFA); then 2 μL of Fe_3O_4@TiO_2 or Fe_3O_4@mTiO_2 was added, and the mixture was incubated at room temperature for 60 min, respectively. After that, Fe_3O_4@TiO_2 or Fe_3O_4@mTiO_2 with captured phosphopeptides was separated from the mixed solutions by applying an external magnet. After washing with 200 μL of loading buffer to remove the nonspecifically adsorbed peptides, the trapped phosphopeptides were eluted with 10 μL of 5% $NH_3 \cdot H_2O$ for further MS analysis.

MALDI Mass Spectrometry. A 1 μL amount of the eluate was deposited on the MALDI probe, and then matrix solution DHB (1 μL) was deposited for MS analysis. MALDI-TOF mass spectrometry analysis was performed in positive reflection mode on a 5800 Proteomic Analyzer (Applied Biosystems, Framingham, MA, USA) with a Nd:YAG laser at 355 nm, a repetition rate of 200 Hz, and an acceleration voltage of 20 kV. The range of laser energy was optimized to obtain good resolution and signal-to-noise ratio (S/N) and kept constant for further analysis. External mass calibration was performed by using standard peptides from myoglobin digests.

Conflict of Interest: The authors declare no competing financial interest.

Acknowledgment. This work was supported by the National Science and Technology Key Project of China (2012CB910602), National Science Foundation of China (Grant No. 20974023, 21025519, 21128001, and 51073040), and the Innovation Foundation for Distinguished Students of Fudan University (11-25-15).

Supporting Information Available: HRTEM image of MCNC; EDX spectrum of Fe_3O_4@TiO_2; The histograms of size distribution of (a) MCNCs, (b) Fe_3O_4@TiO_2, and (c) Fe_3O_4@mTiO_2; magnetic separation behaviors of Fe_3O_4@TiO_2 and Fe_3O_4@mTiO_2 in the enrichment solution; nitrogen adsorption−desorption isotherms of Fe_3O_4@TiO_2; TEM images of Fe_3O_4@mTiO_2 prepared with different hydrothermal treatment time; HRTEM images of Fe_3O_4@mTiO_2 prepared under different $NH_3 \cdot H_2O$MALDI mass spectra of the tryptic digest of β-casein. This material is available free of charge *via* the Internet at http://pubs.acs.org.

REFERENCES AND NOTES

1. Jun, Y. W.; Seo, J. W.; Cheon, A. Nanoscaling Laws of Magnetic Nanoparticles and Their Applicabilities in Biomedical Sciences. *Acc. Chem. Res.* **2008**, *41*, 179–189.
2. Gao, J. H.; Gu, H. W.; Xu, B. Multifunctional Magnetic Nanoparticles: Design, Synthesis, and Biomedical Applications. *Acc. Chem. Res.* **2009**, *42*, 1097–1107.
3. Frey, N. A.; Peng, S.; Cheng, K.; Sun, S. H. Magnetic Nanoparticles: Synthesis, Functionalization, and Applications in Bioimaging and Magnetic Energy Storage. *Chem. Soc. Rev.* **2009**, *38*, 2532–2542.
4. Palchoudhury, S.; An, W.; Xu, Y. L.; Qin, Y.; Zhang, Z. T.; Chopra, N.; Holler, R. A.; Turner, C. H.; Bao, Y. P. Synthesis and Growth Mechanism of Iron Oxide Nanowhiskers. *Nano Lett.* **2011**, *11*, 1141–1146.
5. Deng, Y. H.; Qi, D. W.; Deng, C. H.; Zhang, X. M.; Zhao, D. Y. Superparamagnetic High-Magnetization Microspheres with an Fe_3O_4@SiO_2 Core and Perpendicularly Aligned Mesoporous SiO_2 Shell for Removal of Microcystins. *J. Am. Chem. Soc.* **2008**, *130*, 28–29.
6. Mazzucchelli, S.; Colombo, M.; De Palma, C.; Salvade, A.; Verderio, P.; Coghi, M. D.; Clementi, E.; Tortora, P.; Corsi, F.; Prosperi, D. Single-Domain Protein A-Engineered Magnetic Nanoparticles: Toward a Universal Strategy to Site-Specific Labeling of Antibodies for Targeted Detection of Tumor Cells. *ACS Nano* **2010**, *4*, 5693–5702.
7. Song, E. Q.; Hu, J.; Wen, C. Y.; Tian, Z. Q.; Yu, X.; Zhang, Z. L.; Shi, Y. B.; Pang, D. W. Fluorescent-Magnetic-Biotargeting Multifunctional Nanobioprobes for Detecting and Isolating Multiple Types of Tumor Cells. *ACS Nano* **2011**, *5*, 761–770.
8. Di Corato, R.; Bigall, N. C.; Ragusa, A.; Dorfs, D.; Genovese, A.; Marotta, R.; Manna, L.; Pellegrino, T. Multifunctional Nanobeads Based on Quantum Dots and Magnetic Nanoparticles: Synthesis and Cancer Cell Targeting and Sorting. *ACS Nano* **2011**, *5*, 1109–1121.

9. Sanson, C.; Diou, O.; Thevenot, J.; Ibarboure, E.; Soum, A.; Brulet, A.; Miraux, S.; Thiaudiere, E.; Tan, S.; Brisson, A.; *et al*. Doxorubicin Loaded Magnetic Polymersomes: Theranostic Nanocarriers for MR Imaging and Magneto-Chemotherapy. *ACS Nano* **2011**, *5*, 1122–1140.
10. Luo, B.; Xu, S.; Luo, A.; Wang, W. R.; Wang, S. L.; Guo, J.; Lin, Y.; Zhao, D. Y.; Wang, C. C. Mesoporous Biocompatible and Acid-Degradable Magnetic Colloidal Nanocrystal Clusters with Sustainable Stability and High Hydrophobic Drug Loading Capacity. *ACS Nano* **2011**, *5*, 1428–1435.
11. Sherlock, S. P.; Tabakman, S. M.; Xie, L. M.; Dai, H. J. Photothermally Enhanced Drug Delivery by Ultrasmall Multifunctional FeCo/Graphitic Shell Nanocrystals. *ACS Nano* **2011**, *5*, 1505–1512.
12. Cho, H. S.; Dong, Z. Y.; Pauletti, G. M.; Zhang, J. M.; Xu, H.; Gu, H. C.; Wang, L. M.; Ewing, R. C.; Huth, C.; Wang, F.; *et al*. Fluorescent, Superparamagnetic Nanospheres for Drug Storage, Targeting, and Imaging: A Multifunctional Nanocarrier System for Cancer Diagnosis and Treatment. *ACS Nano* **2010**, *4*, 5398–5404.
13. Jun, Y. W.; Lee, J. H.; Cheon, J. Chemical Design of Nanoparticle Probes for High-Performance Magnetic Resonance Imaging. *Angew. Chem., Int. Ed.* **2008**, *47*, 5122–5135.
14. Ma, L. L.; Feldman, M. D.; Tam, J. M.; Paranjape, A. S.; Cheruku, K. K.; Larson, T. A.; Tam, J. O.; Ingram, D. R.; Paramita, V.; Villard, J. W.; *et al*. Small Multifunctional Nanoclusters (Nanoroses) for Targeted Cellular Imaging and Therapy. *ACS Nano* **2009**, *3*, 2686–2696.
15. Huang, J.; Bu, L. H.; Xie, J.; Chen, K.; Cheng, Z.; Li, X. G.; Chen, X. Y. Effects of Nanoparticle Size on Cellular Uptake and Liver MRI with Polyvinylpyrrolidone-Coated Iron Oxide Nanoparticles. *ACS Nano* **2010**, *4*, 7151–7160.
16. Villanueva, J.; Philip, J.; Entenberg, D.; Chaparro, C. A.; Tanwar, M. K.; Holland, E. C.; Tempst, P. Serum Peptide Profiling by Magnetic Particle-Assisted, Automated Sample Processing and MALDI-TOF Mass Spectrometry. *Anal. Chem.* **2004**, *76*, 1560–1570.
17. Bao, J.; Chen, W.; Liu, T. T.; Zhu, Y. L.; Jin, P. Y.; Wang, L. Y.; Liu, J. F.; Wei, Y. G.; Li, Y. D. Bifunctional Au-Fe_3O_4 Nanoparticles for Protein Separation. *ACS Nano* **2007**, *1*, 293–298.
18. Tan, F.; Zhang, Y.; Mi, W.; Wang, J.; Wei, J.; Cai, Y.; Qian, X. Enrichment of Phosphopeptides by Fe^{3+}-Immobilized Magnetic Nanoparticles for Phosphoproteome Analysis of the Plasma Membrane of Mouse Liver. *J. Proteome Res.* **2008**, *7*, 1078–1087.
19. Deng, Y. H.; Deng, C. H.; Qi, D. W.; Liu, C.; Liu, J.; Zhang, X. M.; Zhao, D. Y. Synthesis of Core/Shell Colloidal Magnetic Zeolite Microspheres for the Immobilization of Trypsin. *Adv. Mater.* **2009**, *21*, 1377–1382.
20. Chen, H. M.; Deng, C. H.; Zhang, X. M. Synthesis of Fe_3O_4@SiO_2@PMMA Core-Shell-Shell Magnetic Microspheres for Highly Efficient Enrichment of Peptides and Proteins for MALDI-ToF MS Analysis. *Angew. Chem., Int. Ed.* **2010**, *49*, 607–611.
21. Liu, S. S.; Chen, H. M.; Lu, X. H.; Deng, C. H.; Zhang, X. M.; Yang, P. Y. Facile Synthesis of Copper(II) Immobilized on Magnetic Mesoporous Silica Microspheres for Selective Enrichment of Peptides for Mass Spectrometry Analysis. *Angew. Chem., Int. Ed.* **2010**, *49*, 7557–7561.
22. Ptacek, J.; Devgan, G.; Michaud, G.; Zhu, H.; Zhu, X. W.; Fasolo, J.; Guo, H.; Jona, G.; Breitkreutz, A.; Sopko, R.; *et al*. Global Analysis of Protein Phosphorylation in Yeast. *Nature* **2005**, *438*, 679–684.
23. Olsen, J. V.; Blagoev, B.; Gnad, F.; Macek, B.; Kumar, C.; Mortensen, P.; Mann, M. Global, *in Vivo*, and Site-Specific Phosphorylation Dynamics in Signaling Networks. *Cell* **2006**, *127*, 635–648.
24. Huttlin, E. L.; Jedrychowski, M. P.; Elias, J. E.; Goswami, T.; Rad, R.; Beausoleil, S. A.; Villen, J.; Haas, W.; Sowa, M. E.; Gygi, S. P. A Tissue-Specific Atlas of Mouse Protein Phosphorylation and Expression. *Cell* **2010**, *143*, 1174–1189.
25. Thingholm, T. E.; Jorgensen, T. J. D.; Jensen, O. N.; Larsen, M. R. Highly Selective Enrichment of Phosphorylated Peptides Using Titanium Dioxide. *Nat. Protoc.* **2006**, *1*, 1929–1935.
26. Nelson, C. A.; Szczech, J. R.; Xu, Q. G.; Lawrence, M. J.; Jin, S.; Ge, Y. Mesoporous Zirconium Oxide Nanomaterials Effectively Enrich Phosphopeptides for Mass Spectrometry-Based Phosphoproteomics. *Chem. Commun.* **2009**, *43*, 6607–6609.
27. Nelson, C. A.; Szczech, J. R.; Dooley, C. J.; Xu, Q.; Lawrence, M. J.; Zhu, H.; Jin, S.; Ge, Y. Effective Enrichment and Mass Spectrometry Analysis of Phosphopeptides Using Mesoporous Metal Oxide Nanomaterials. *Anal. Chem.* **2009**, *82*, 7193–7201.
28. Lu, Z. D.; Ye, M. M.; Li, N.; Zhong, W. W.; Yin, Y. D. Self-Assembled TiO_2 Nanocrystal Clusters for Selective Enrichment of Intact Phosphorylated Proteins. *Angew. Chem., Int. Ed.* **2010**, *49*, 1862–1866.
29. Lu, Z. D.; Duan, J. C.; He, L.; Hu, Y. X.; Yin, Y. D. Mesoporous TiO_2 Nanocrystal Clusters for Selective Enrichment of Phosphopeptides. *Anal. Chem.* **2010**, *82*, 7249–7258.
30. Yan, J. Y.; Li, X. L.; Yu, L.; Jin, Y.; Zhang, X. L.; Xue, X. Y.; Ke, Y. X.; Liang, X. M. Selective Enrichment of Glycopeptides/Phosphopeptides Using Porous Titania Microspheres. *Chem. Commun.* **2010**, *46*, 5488–5490.
31. Liu, J.; Sun, Z. K.; Deng, Y. H.; Zou, Y.; Li, C. Y.; Guo, X. H.; Xiong, L. Q.; Gao, Y.; Li, F. Y.; Zhao, D. Y. Highly Water-Dispersible Biocompatible Magnetite Particles with Low Cytotoxicity Stabilized by Citrate Groups. *Angew. Chem., Int. Ed.* **2009**, *48*, 5875–5879.
32. Ma, W. F.; Xu, S.; Li, J. M.; Guo, J.; Lin, Y.; Wang, C. C. Hydrophilic Dual-Responsive Magnetite/PMAA Core/Shell Microspheres with High Magnetic Susceptibility and pH Sensitivity *via* Distillation-Precipitation Polymerization. *J. Polym. Sci., Part A: Polym. Chem.* **2011**, *49*, 2725–2733.
33. Wang, P.; Chen, D.; Tang, F. Q. Preparation of Titania-Coated Polystyrene Particles in Mixed Solvents by Ammonia Catalysis. *Langmuir* **2006**, *22*, 4832–4835.
34. Shen, Z. Y.; Li, L. Y.; Li, Y.; Wang, C. C. Fabrication of Hydroxyl Group Modified Monodispersed Hybrid Silica Particles and the h-SiO_2/TiO_2 Core/Shell Microspheres As High Performance Photocatalyst for Dye Degradation. *J. Colloid Interface Sci.* **2011**, *354*, 196–201.
35. Chen, W. J.; Tsai, P. J.; Chen, Y. C. Functional Fe_3O_4/TiO_2 Core/Shell Magnetic Nanoparticles As Photokilling Agents for Pathogenic Bacteria. *Small* **2008**, *4*, 485–491.
36. Wang, C. X.; Yin, L. W.; Zhang, L. Y.; Kang, L.; Wang, X. F.; Gao, R. Magnetic (γ-Fe_2O_3@SiO_2)n @TiO_2 Functional Hybrid Nanoparticles with Actived Photocatalytic Ability. *J. Phys. Chem. C* **2009**, *113*, 4008–4011.
37. Ye, M. M.; Zhang, Q.; Hu, Y. X.; Ge, J. P.; Lu, Z. D.; He, L.; Chen, Z. L.; Yin, Y. D. Magnetically Recoverable Core-Shell Nanocomposites with Enhanced Photocatalytic Activity. *Chem.—Eur. J.* **2010**, *16*, 6243–6250.
38. Ge, J. P.; Hu, Y. X.; Biasini, M.; Beyermann, W. P.; Yin, Y. D. Superparamagnetic Magnetite Colloidal Nanocrystal Clusters. *Angew. Chem., Int. Ed.* **2007**, *46*, 4342–4345.
39. Chen, L. S.; Yang, R. T. Improved Horvath-Kawazoe Equations Including Spherical Pore Models For Calculating Micropore Size Distribution. *Chem. Eng. Sci.* **1994**, *49*, 2599–2609.
40. Yu, J. G.; Su, Y. R.; Cheng, B.; Zhou, M. H. Effects of pH on the Microstructures and Photocatalytic Activity of Mesoporous Nanocrystalline Titania Powders Prepared *via* Hydrothermal Method. *J. Mol. Catal. A: Chem.* **2006**, *258*, 104–112.
41. Gelb, L. D.; Gubbins, K. E. Characterization of Porous Glasses: Simulation Models, Adsorption Isotherms, and the Brunauer-Emmett-Teller Analysis Method. *Langmuir* **1998**, *14*, 2097–2111.
42. Ojeda, M. L.; Esparza, J. M.; Campero, A.; Cordero, S.; Kornhauser, I.; Rojas, F. on Comparing BJH and NLDFT Pore-Size Distributions Determined from N_2 Sorption on SBA-15 Substrata. *Phys. Chem. Chem. Phys.* **2003**, *5*, 1859–1866.
43. Larsen, M. R.; Jensen, S. S.; Jakobsen, L. A.; Heegaard, N. H. H. Exploring the Sialiome Using Titanium Dioxide

Chromatography and Mass Spectrometry. *Mol. Cell. Proteomics* **2007**, *6*, 1778–1787.
44. Chen, C. T.; Chen, Y. C. Trapping Performance of Fe_3O_4@Al_2O_3 and Fe_3O_4@TiO_2 Magnetic Nanoparticles in the Selective Enrichment of Phosphopeptides from Human Serum. *J. Biomed. Nanotechnol.* **2008**, *4*, 73–79.
45. Li, Y.; Wu, J. S.; Qi, D. W.; Xu, X. Q.; Deng, C. H.; Yang, P. Y.; Zhang, X. M. Novel Approach for the Synthesis of Fe_3O_4@TiO_2 Core−Shell Microspheres and Their Application to the Highly Specific Capture of Phosphopeptides for MALDI-TOF MS Analysis. *Chem. Commun.* **2008**, *5*, 564–566.
46. Li, Y.; Xu, X. Q.; Qi, D. W.; Deng, C. H.; Yang, P. Y.; Zhang, X. M. Novel Fe_3O_4@TiO_2 Core-Shell Microspheres for Selective Enrichment of Phosphopeptides in Phosphoproteome Analysis. *J. Proteome Res.* **2008**, *7*, 2526–2538.
47. Yao, X. D.; Freas, A.; Ramirez, J.; Demirev, P. A.; Fenselau, C. Proteolytic ^{18}O Labeling for Comparative Proteomics: Model Studies with Two Serotypes of Adenovirus. *Anal. Chem.* **2001**, *73*, 2836–2842.